I&EC research
Industrial & Engineering Chemistry Research

Article

Cite This: Ind. Eng. Chem. Res. 2018, 57, 15375−15384

pubs.acs.org/IECR

Influence of Al Coordinates on Hierarchical Structure and T Atoms Redistribution during Base Leaching of ZSM-5

Junjie Li,[†] Min Liu,*[,†] Xinwen Guo,[†] Shu Zeng,[‡,§] Shutao Xu,[§] Yingxu Wei,[§] Zhongmin Liu,[§] and Chunshan Song*[,†,∥]

[†]State Key Laboratory of Fine Chemicals, PSU-DUT Joint Center for Energy Research, School of Chemical Engineering, Dalian University of Technology, Dalian 116024, People's Republic of China

[‡]University of Chinese Academy of Sciences, Beijing 100049, People's Republic of China

[§]State Key Laboratory of Catalysis, Dalian Institute of Chemical Physics, Chinese Academy of Sciences, Dalian 116023, People's Republic of China

[∥]Department of Energy and Mineral Engineering, EMS Energy Institute, PSU-DUT Joint Centre for Energy Research, Pennsylvania State University, University Park, Pennsylvania 16802, United States

Supporting Information

ABSTRACT: Al coordinates in ZSM-5 showed significant effects on hierarchical structure and T atoms redistribution during NaOH/TPAOH treatment and different catalytic performances in the methanol-to-propylene reaction. NaOH treatment of parent ZSM-5 with a few extra-framework Al sites mainly involved the desilication process, while an additional alumination process was observed when some Al^{3+} was added into the NaOH solution, which resulted in mesoporous crystals with intact outer shells. Dealumination−realumination and desilication processes occurred with ZSM-5 with distorted four-coordinate, five-coordinate, or six-coordinate Al sites. For TPAOH treatment, the desilication−recrystallization process occurred with parent ZSM-5 and resulted in hollow crystals with ultrasilica shells via Si redistribution, consequently 2.5 times the lifetime of parent ZSM-5 by restricting external coke deposition. By comparison, desilication, dealumination, and (Si, Al)-recystallization were observed for ZSM-5 with distorted four-coordinate Al sites, involving both Si and Al atoms redistribution processes resulting in abundant mesopores and a high-silica outer surface, which showed almost 5 times the lifetime of parent ZSM-5.

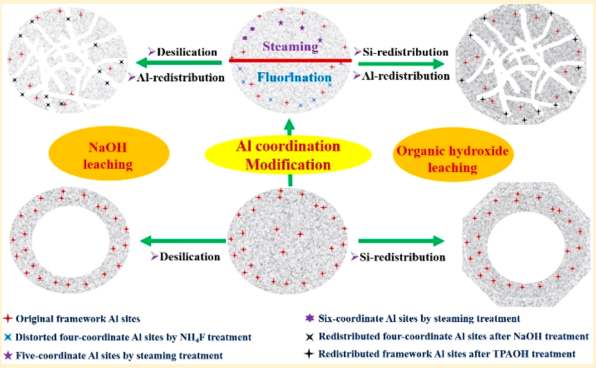

1. INTRODUCTION

Zeolites have been widely used in separation and petrochemical fields, which benefits from their high thermal/hydrothermal stabilities, high surface area, and intrinsic acidity, especially shape selectivity from microporous structures.[1−7] However, intrinsic micropores significantly restrict diffusion of reactants and products, which gives rise to low activity and stability in the reactions involving large molecules.[8] Ordered mesoporous materials (e.g., MCM-41, SBA-15, etc.) with amorphous walls show limited application because of low thermal/hydrothermal stabilities and weak acidity.[9−11] Nanocrystals with short diffusion paths enhance diffusion greatly, but it shows some difficulties in synthesis and separation.[8,12−14] Development of microporous materials with large micropores in the range between 1 and 2 nm, by using Ge as a costructure directing agent, enhances diffusion, but low thermal stability and high cost restrict their applications.[15,16] Introducing additional mesoporous structures into zeolites has been proven to be an efficient method to take advantage of microporous and mesoporous materials.[17−19]

As is known, there are two main approaches for obtaining hierarchical zeolites. The first one is the templating method, which can be divided into three main classes: (I) soft templating, includes amphiphilic organosilanes and polyquaternary ammonium-form surfactants that orient to nanocrystals aggregate and lamellar crystal, respectively;[20−25] (II) hard templating, the carbon materials (e.g., carbon blacks, carbon nanotube, carbon nanofibers, etc.), aerogel, polymer, or resin is added into the synthesis gel, and then the mesoporous structure is obtained after high-temperature combustion;[26−31] (III) indirect templating, hierarchical structure is produced by partial transformation of amorphous walls of mesoporous materials into crystalline ones or by supporting nanozeolites crystals onto the walls.[32] However, required costly templates and synthesis difficulties restrict large-scale applications of

Received: July 29, 2018
Revised: October 16, 2018
Accepted: October 22, 2018
Published: October 22, 2018

DOI: 10.1021/acs.iecr.8b03539
Ind. Eng. Chem. Res. 2018, 57, 15375−15384

templating methods. By contrast, introducing mesoporous structures into microporous materials, via postsynthesis methods, shows great potential in industrial applications.[19,33] Dealumination by a steaming treatment at high temperature or acid leaching is a common method to prepare USY. Some enclosed mesoporous structures are introduced after treatment,[34] but it is impracticable for zeolites with high Si/Al. Recently, the so-called "desilication" method, which preferentially extracts silica from the zeolites matrix to the alkaline solution, has been proven to be a much more efficient method for introducing additional mesopores into ZSM-5, Beta, ZSM-22, ZSM-11, MCM-22, Y, and so on. Desilication has been successfully scaled up to kilogram-scale for commercial catalysts in powder or extrudate form.[35,36]

Numerous works have been employed since the original work in 2000 by Matsukata and co-workers.[37] Peréz-Ramírez et al. demonstrated that Al (B, Fe, or Ga) served as pore directing agents for mesopore formation.[38,39] Alkaline treatment of ZSM-5 with lower Si/Al resulted in a few mesopores, because of excessive protection effects of large amounts of Al sites to neighbor Si.[38] Sequential treatment of acid-washing-desilication or fluorination-deslication was used to construct mesopores in ZSM-5 with lower Si/Al;[40,41] while large pores and low solid yield were achieved for ZSM-5 with high Si/Al, because of uncontrollable dissolution during alkaline treatment, which can be solved by adding TPA^+, TBA^+, CTAB, or piperidine in the alkaline solution.[42−45] Hierarchical zeolites have been widely used in heterogeneous catalysis reactions, like MTH, biomass transformation, catalytic cracking, isomerization, etc.[8,12] However, there are still some problems that remain to be solved before industrial application, one of which is the influence of various Al coordinates on alkaline treatment, especially on hierarchical structure and T atoms redistribution. Besides, the solid yield after desilication was lower than 70%, and the obtained mesoporous zeolites via alkaline treatment exhibited lower crystallinity and localized amorphization.[46−49]

In this study, ZSM-5 with various Al species (intrinsic framework four-coordinate Al, five/six-coordinate Al by steaming treatment, distorted four-coordinate Al by fluorination, and Al^{3+} from $Al(NO_3)_3$ solution) was treated with the NaOH solution at 353 K. ZSM-5 with only framework Al and modified ZSM-5 with a part of distorted four-coordinate Al were treated by 0.3 mol/L TPAOH at 443 K. The products with different hierarchical structures were characterized by XRD, SEM, TEM, and physisorption. Redistribution of T atoms was studied by ICP, XPS, XRF, NH_3-TPD, OH-IR, 2,6-di-*tert*-butylpyridine IR, ^{27}Al MAS NMR, and ^{29}Si MAS NMR. ZSM-5 with various hierarchical structure and T atoms distribution was evaluated in the MTP reaction.

2. EXPERIMENTAL SECTION

2.1. Catalysts Preparation. All samples with simple annotations are listed in the Supporting Information.

Sample Z1 was synthesized as follows. 17.75 g of TPABr and 1.04 g of seed suspension comprised 0.5 wt % nano silicate-1 (with uniform particle size at around 60−70 nm) were added into 66.67 g of colloidal silica solution (30 wt % in H_2O), and the mixture was labeled as solution A. After a 30-min hydrolysis at 308 K, a solution containing 2.07 g of $AlCl_3 \cdot 6H_2O$ and 45 g of H_2O was added dropwise into solution A. Finally, 22.26 g of ethylamine aqueous solution (65 wt % in H_2O) was poured into the above mixture. The obtained gel was crystallized at 443 K for 72 h. The molar composition of the final gel was 1 SiO_2:0.0125 Al_2O_3:0.20 TPABr:1 ethylamine:17 H_2O. The solid product was collected by centrifugation and drying overnight at 373 K, following by a calcination step at 813 K for 6 h.

Sample Z2 was synthesized via a previous method.[50] 24.22 g of TEOS (tetraethyl orthosilicate) was added into a solution containing 90 g of H_2O and 23.26 g of TPAOH (25 wt % in H_2O). After hydrolysis at 308 K for 8 h, a solution containing 1.09 g of $Al(NO_3)_3 \cdot 9H_2O$ and 0.46 g of NaOH was added into the mixture. This mother gel was crystallized at 443 K for 24 h. The solid product was collected by centrifugation and drying overnight at 373 K, following by a calcination step at 813 K for 6 h to remove the template.

Fluorination was performed by dispersing 10 g of powder into 200 mL of 0.06 mol/L NH_4F solution, following by vigorous stirring at 303 K for 10 h; after that, the suspension was evaporated at 373 K. Finally, NH_4F modification was completed after calcination at 873 K for 6 h. NH_4F treated sample Z1 or Z2 was denoted as Z1-F or Z2-F. Steaming treatment was performed in a fixed-bed continuous-flow reactor, 10 g of catalyst (size 10−20 mesh) was loaded in the middle section of the reactor, and 100% H_2O (WHSV = 2 h^{-1}) was injected by a Lab Alliance Series II pump. The treatment was conducted at 823 K for 3.5 h, and the treated sample was labeled as Z1-Steam.

NaOH treatment was performed at 353 K. Ten g of Z1, Z1-F, or Z1-Steam was dispersed into 300 mL of 0.2 mol/L sodium hydroxide solution. The suspension was immediately quenched in ice water after 30 min, and Z1-AT1, Z1-F-AT1, or Z1-Steam-AT1 was obtained by centrifugation, washing with distilled water, and drying at 373 K overnight. NaOH treatment of Z1 with additive 0.0060 mol/L $Al(NO_3)_3 \cdot 9H_2O$ was labeled as Z1-AT2. TPAOH treatment was performed at 443 K for 72 h. Four g of Z2 or Z2-F was dispersed into 60 mL of 0.3 mol/L TPAOH solution, then transferred into a 100 mL Teflon-lined stainless-steel autoclave, and heated in a rotating autoclave. The solid products were calcined at 813 K for 6 h to remove TPA^+ and denoted as Z2-AT3 and Z2-F-AT3, respectively. Characterization and evaluation in the MTP reaction were operated on H-form ZSM-5.

2.2. Catalysts Characterization. X-ray diffraction (XRD) measurement was performed on a RIGAKU D/Max 2400 apparatus with a Cu Kα X-radiation (1.542 Å). An X-ray photoelectron spectroscopy (XPS) apparatus (Escalab 250) was used to analyze external chemical compositions of different samples. The field-emission scanning electron microscopy (SEM) images were taken on a cold field emission Hitachi SU8200 instrument. TEM images were obtained on a Tecnai G2 20 S-twin instrument (FEI Company). Argon adsorption−desorption was measured in a Quantachrome autosorb Q2 gas adsorption analyzer at 87 K, and nitrogen adsorption−desorption isotherms were recorded on a Quadrasorb SI gas analyzer at 77 K. Before the measurements, samples were degassed at 573 K for 10 h. The elemental analysis of catalysts was conducted on a PerkinElmer OPTIMA 2000DV ICP optical emission spectrometer. X-ray fluorescence (XRF) spectroscopy on a SRS-3400 X-ray fluorometer was used to analyze the chemical compositions of different samples. Infrared spectroscopy with 2,6-di-*tert*-butylpyridine adsorption was carried out using an EQUINOX55 Fourier transform infrared spectrometer (FT-IR) (Bruker Corp.), and the samples were desorbed under vacuum at 423 K for 15 min. The OH-IR spectra were obtained by means of the KBr pellet

DOI: 10.1021/acs.iecr.8b03539
Ind. Eng. Chem. Res. 2018, 57, 15375−15384

technique. Prior to the measurements, the samples were heated to 573 K under vacuum (1.33×10^{-3} Pa) for 1 h. The spectra of all samples were presented by subtracting the background spectrum.

Ammonium temperature-programmed desorption (NH_3-TPD) profiles were obtained on a CHEMBET 3000 absorber. All of the samples were pretreated at 773 K for 1 h in helium and then cooled to 393 K. About 100 mg of 20−40 mesh samples was exposed to NH_3 atmosphere for 0.5 h; in order to remove physically adsorbed NH_3, the samples were purged by helium flow at 393 K for 1 h. NH_3-TPD was performed in the temperature range 393−923 K at a rate of 10 K/min. Chemisorbed NH_3 was monitored by a TCD detector.

^{29}Si and ^{27}Al MAS NMR experiments were conducted on a 600 MHz Bruker Avance III spectrometer. ^{29}Si MAS NMR spectra were recorded using high-power proton decoupling at a spinning rate of 10 kHz. 1024 scans were accumulated with a $\pi/2$ pulse width of 3 μs and a recycle delay of 10 s. ^{27}Al MAS NMR spectra were recorded using one pulse sequence at a spinning rate of 12 kHz. 200 scans were accumulated with a $\pi/8$ pulse width of 0.75 μs and a recycle delay of 2 s.

2.3. Catalytic Reaction. Methanol-to-propylene (MTP) reactions were carried out on a fixed-bed reactor. Prior to reaction, 1 g of sieved catalyst with 10−20 mesh was loaded in the reactor and then activated at 773 K for an hour under N_2 flow. A high performance liquid chromatography pump was used to feed methanol−water into the reactor system with a methanol WHSV of 3.4 h^{-1}. The molar ratio of methanol to water was 1:1. Reaction was operated at 773 K and atmospheric pressure; the products distribution was determined by off-line analysis on a gas chromatograph. Dimethyl ether also served as a reactant as well as methanol for conversion calculation.

3. RESULTS AND DISCUSSION

3.1. Influence of Various Al Coordinates during NaOH Treatment. Parent Z1, steamed Z1-Steam, and fluorinated Z1-F with various Al coordinates (Figure S1) were treated separately with the NaOH solution. XRD patterns of alkaline treated samples are shown in Figure 1. All of the samples

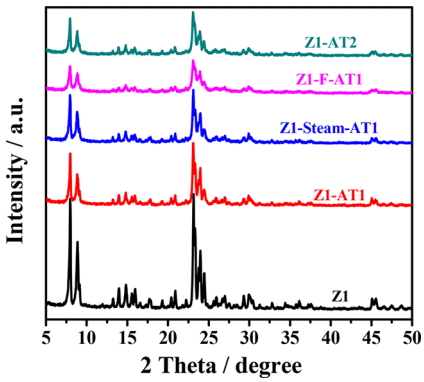

Figure 1. XRD patterns of samples via different treatment methods.

exhibited typical MFI topology. However, the crystallinity reduced significantly after alkaline treatment for Z1-AT1, Z1-F-AT1, Z1-Steam-AT1, and Z1-AT2, comparing with parent Z1.

As it is known that NaOH treatment of ZSM-5 selectively removed Si sites, including defective Si sites and framework Si sites, how about Al sites? The variation of Al contents in the NaOH solution as treatment time extension is shown in Figure 2. It exhibited low concentration of Al in the filtration

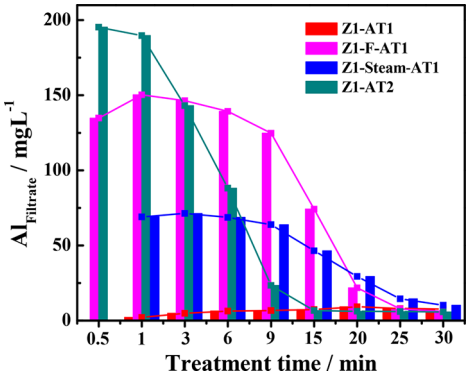

Figure 2. Al concentration in the alkaline solution for Z1-AT1, Z1-F-AT1, Z1-Steam-AT1, and Z1-AT2 as treatment time extension.

throughout the NaOH treatment for parent Z1. Thus, it can be concluded that framework four-coordinate Al sites were difficult to extract out by OH^-. By contrast, many more Al sites were leached out by NaOH in the initial 1 min for Z1-F-AT1, and there was also a higher concentration of Al in the alkaline solution for Z1-Steam-AT1 with five-/six-coordinate Al species. Generally speaking, distorted four-coordinate Al sites and five-/six-coordinate Al sites could be leached out during alkaline treatment, differing from framework four-coordinate Al sites. Interestingly, there was lower concentration of Al retaining in the final solution after 30 min, regardless of how many Al sites were extracted out in the initial stage, which indicated a realumination process during alkaline treatment, and NaOH treatment with additive $Al(NO_3)_3$ (Z1-AT2) exhibited a similar Al deposition process (alumination) with prolonged treatment time.

The influence of Al coordinates on hierarchical structure was studied by SEM and TEM. As shown in Figure 3, the SEM (**A1**) and TEM (**A2**) images of the Z1-AT1 sample displayed crystals with larger pores, along with a lower solid yield of 47% in Table 1. By contrast, uniform smaller mesopores were observed for Z1-Steam-AT1 (**B1** and **B2**), with a higher solid yield of 66%. Alkaline treatment of the fluorinated sample (Z1-F-AT1) resulted in similar morphology and pore structure (SEM and TEM, **C1** and **C2**) as Z1-Steam-AT1 and a higher solid yield of 64% (Table 1), while a crystal with an interior mesoporous structure and a relatively protected outer shell was obtained via NaOH treatment with additive $Al(NO_3)_3$ (Z1-AT2, **D1** and **D2**).

N_2 adsorption was employed to characterize the hierarchical structures. As shown in Figure 4a, all of the samples displayed type IV adsorption−desorption isotherms, typical for microporous materials with additional mesopores or macropores. Nevertheless, the samples showed different hysteresis loops that indicated various mesoporous structures.[48,51] The pore distribution of different samples is shown in Figure 4b. Z1-AT1 exhibited nonuniform mesopores, along with certain amounts of macropores. By comparison, Z1-F-AT1 and Z1-Steam-AT1 displayed uniform mesopores centered at ∼12 nm and ∼9 nm, respectively. Z1-AT1, Z1-F-AT1, and Z1-Steam-AT1 displayed similar mesoporous volume (Table 1), but Z1-Steam-AT1, Z1-F-AT1, and Z1-AT2 exhibited larger external surface area compared with Z1-AT1.

DOI: 10.1021/acs.iecr.8b03539
Ind. Eng. Chem. Res. 2018, 57, 15375−15384

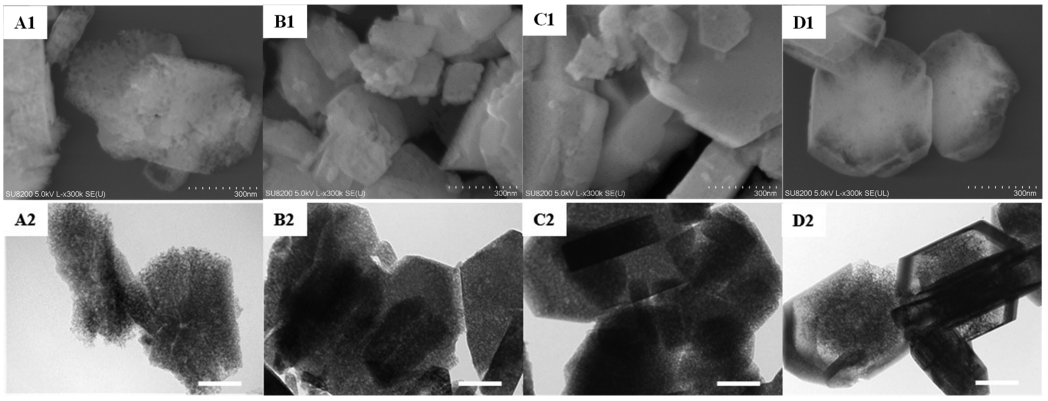

Figure 3. SEM and TEM images of NaOH treated samples: (**A1**, **A2**), sole NaOH treatment (Z1-AT1); (**B1**, **B2**), sequential steaming and NaOH treatment (Z1-Steam-AT1); (**C1**, **C2**), sequential fluorination and NaOH treatment (Z1-F-AT1); and (**D1**, **D2**), NaOH treatment with additional $Al(NO_3)_3$ (Z1-AT2). **C1** and **C2** came from our previous study.[50]

Table 1. Textural Properties of Z1-AT1, Z1-Steam, Z1-F-AT1, and Z1-AT2 Samples

samples	S_{BET}[a] (m^2/g)	S_{Meso}[b] (m^2/g)	V_T[c] (cm^3/g)	V_{Micro}[d] (cm^3/g)	V_{Meso}[e] (cm^3/g)	yield[f] (%)
Z1-AT1	386	79	0.44	0.13	0.31	47
Z1-Steam-AT1	409	151	0.40	0.11	0.29	66
Z1-F-AT1	402	133	0.41	0.11	0.30	64
Z1-AT2	410	125	0.47	0.12	0.35	60

[a]S_{BET} calculated by the BET method. [b]S_{Meso} measured by the T-plot method. [c]V_T was determined by N_2 adsorption volume at $P/P_0 = 0.99$. [d]V_{Micro} measured by the T-plot method. [e]$V_{Meso} = V_T - V_{Micro}$. [f]Yield = M_a/M; M_a was the mass after alkaline treatment, and M was the mass before treatment.

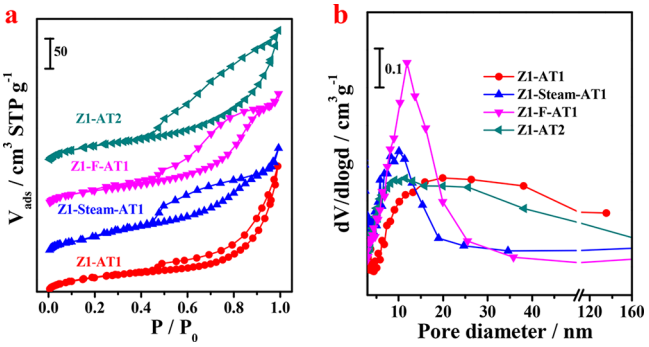

Figure 4. N_2 adsorption−desorption isotherms (**a**) and pore distribution curves (**b**) of Z1-AT1, Z1-Steam-AT1, Z1-F-AT1, and Z1-AT2 samples.

In summary, NaOH treatment of parent Z1 mainly involved the desilication process, leading to lower solid yield and larger pores. A distinct alumination process was observed for NaOH treatment with additive 0.006 mol/L $Al(NO_3)_3$ besides the desilication process, which led to mesoporous crystals with an excess protected outer surface, and higher solid yield. Dealumination-realumination (Al redistribution) and desilication processes occurred for modified samples with a part of removable Al sites during NaOH treatment, which resulted in uniform mesopores and relatively higher solid yield. As shown in Figure S2 and Table S1, Z1-AT1 showed similar acidity with parent Z1, while larger amounts of medium acid sites were generated for Z1-AT2. Z1-F-AT1 and Z1-Steam-AT1 displayed fewer acid sites compared with parent Z1, which indicated that those redistributed Al sites by the dealumination-realumination process contributed less to acidity.

3.2. Influence of Various Al Coordinates during TPAOH Treatment. TPAOH treatment at higher temperature (443 K) involved an additional recrystallization process compared with NaOH treatment.[52,53] Based on the above-mentioned results, ZSM-5 (Z2) with only framework Al sites (^{27}Al MAS NMR results, Figure S3) may only involve desilication and Si-recrystallization processes; while dealumination, desilication, and (Si, Al)-recrystallization processes may occur with fluorinated ZSM-5 (Z2-F) with a part of the distorted four-coordinate Al sites simultaneously. Thus, samples with various hierarchical structure and distinct T atoms regional distribution will be obtained after TPAOH treatment.

3.2.1. Influence on Hierarchical Structure. Figure 5 shows XRD patterns of parent Z2, fluorinated Z2-F, TPAOH treated

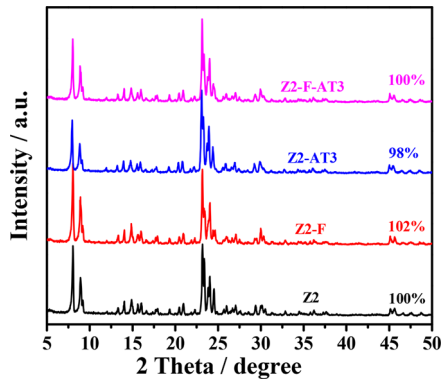

Figure 5. XRD patterns of parent Z2, TPAOH treated Z2-AT3, fluorinated Z2-F, and Z2-F-AT3 via sequential fluorination and TPAOH treatment.

Z2-AT3, and Z2-F-AT3. All of the samples displayed typical MFI topology with similar crystallinity, which was different from conventional NaOH treatment, because of the additional recrystallization process. A higher solid yield of 91% for Z2-AT3 and Z2-F-AT3 (Table 2) also demonstrated the recrystallization process during TPAOH treatment. SEM and TEM results are shown in Figure 6. The SEM and TEM images (**A1** and **A2**) of parent Z2 displayed coffin-like crystals with less mesoporous structures. Z2-AT3 showed a hollow

DOI: 10.1021/acs.iecr.8b03539
Ind. Eng. Chem. Res. 2018, 57, 15375−15384

Table 2. Textual Properties of Parent Z2 and TPAOH Treated Samples

sample	Si/Al[a]	Si/Al[b]	S_{BET}[c]	S_{Meso}[d]	V_T[e]	V_{Micro}[f]	V_{Meso}[g]	yield[h]
Z2	37	41	519	14	0.28	0.19	0.03	100
Z2-F	35	80	513	11	0.35	0.19	0.04	99
Z2-AT3	33	35	493	28	0.42	0.18	0.06	91
Z2-F-AT3	33	35	510	101	0.55	0.18	0.25	91

[a]Bulk Si/Al by XRF results. [b]Framework Si/Al by ^{29}Si MAS NMR spectra. [c]By the BET method. [d]By cumulative surface area between 2 and 50 nm. [e]P/P_0 = 0.99. [f]The SF method. [g]By cumulative mesopore volume between 2 and 50 nm. [h]M_a/M; M_a was the mass after TPAOH treatment, and M was the mass before treatment.

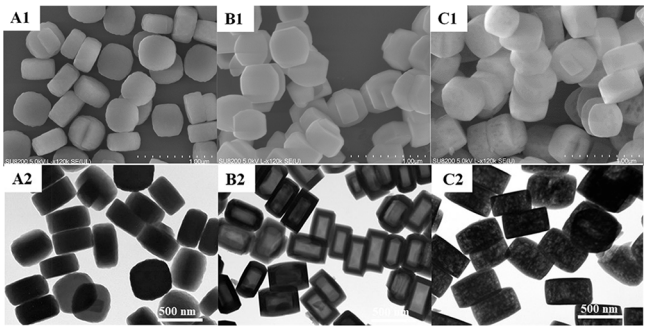

Figure 6. SEM and TEM images of different samples: (**A1**, **A2**), parent Z2; (**B1**, **B2**), TPAOH treated Z2-AT3; and (**C1**, **C2**), sequential NH_4F and TPAOH treated Z2-F-AT3.

structure with an intact outer shell (**B1** and **B2**). By contrast, the mesoporous structure was achieved for Z2-F-AT3 (**C1** and **C2**). Ar adsorption results in Figure S4 were helpful to analyze the pore structure. Z2-AT3 displayed an apparent H2 hysteresis that indicated an enclosed hollow structure combined with TEM results. As shown in Table 2, Z2-AT3 showed a slightly higher mesoporous surface area (28 m^2/g) compared with Z2 (14 m^2/g), while obvious Ar adsorption at higher partial pressure (P/P_0) was observed for Z2-F-AT3 that represented larger amounts of mesopores. It exhibited a higher mesoporous surface area of 101 m^2/g and a higher mesoporous volume of 0.25 cm^3/g compared with Z2-AT3 (0.06 cm^3/g).

3.2.2. Influence on Acid Property. NH_3-TPD results were employed to characterize acid properties of different samples. As shown in Figure 7a, there were two NH_3 desorption peaks. The first peak at a relatively lower temperature was attributed to weak acid sites, and the second peak at a relatively higher temperature belonged to strong acid sites. Z2-F via NH_4F modification exhibited smaller peaks at both low and high temperature, which demonstrated less weak and strong acid sites of Z2-F. As previous studies reported,[50,54] fluorination turned a part of framework Al sites into distorted four-coordinate Al sites that contributed less to acidity, and it displayed a higher framework Si/Al ratio of 80 compared with parent Z2 (Figure S5 and Table 2). Z2-AT3 exhibited slightly larger amounts of weak and strong acid sites compared with parent Z2, while greatly increased weak and strong acid sites were achieved after TPAOH treatment of Z2-F (Z2-F-AT3), which indicated that those distorted four-coordinate Al sites in sample Z2-F may be transformed into framework Al sites during TPAOH treatment.

OH-IR spectra were also employed for further study of the acid property. There were four main bands in OH-IR spectra (Figure 7b). The bands at 3500 and 3720 cm^{-1} were attributed to silanol nests and internal silanol groups, respectively. Both of them were defective sites. The band at 3735 cm^{-1} belonged to external silanol groups, and the last band at 3600 cm^{-1} was attributed to framework aluminum hydroxyl.[55] The spectrum of parent Z2 displayed larger bands at 3500 and 3720 cm^{-1}, pointing to large amounts of defective sites. The bands at 3500 and 3720 cm^{-1} disappeared for Z2-F, because of selective removal of defective sites via fluorination.[54,56] Besides, it exhibited a smaller band at 3600 cm^{-1} that represented fewer framework Al sites compared with Z2. The spectra of TPAOH treated Z2-AT3 and Z2-F-AT3 showed no band at 3500 cm^{-1}, indicative of fewer defective sites, because of selective removal of defective Si sites during TPAOH treatment. The spectrum of Z2-AT3 displayed a slightly larger peak at 3600 cm^{-1} that represented slightly larger amounts of framework Al sites compared with Z2. A larger band at 3600 cm^{-1} was also observed for Z2-F-AT3 via sequential fluorination and TPAOH treatment compared with Z2-F, which indicated that large amounts of framework Al sites were created after TPAOH treatment, and the spectrum of Z2-F-AT3 displayed the largest band at 3735 cm^{-1} that corresponded to the largest mesoporous surface area (Table 2). ^{29}Si MAS NMR spectra are shown in Figure 8. Parent Z2 displayed a framework Si/Al of 41 that was similar to bulk Si/Al (XRF results, Table 2); in other words, nearly all Al sites were determined as framework four-coordinate Al species. TPAOH treated Z2-AT3 and Z2-F-AT3 displayed the same lower framework Si/Al of 35

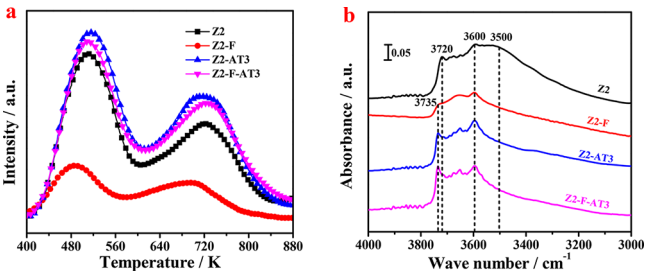

Figure 7. **a**. NH_3-TPD profiles of parent Z2 and postsynthesized samples and **b**. FT-IR spectra in the OH region for different samples.

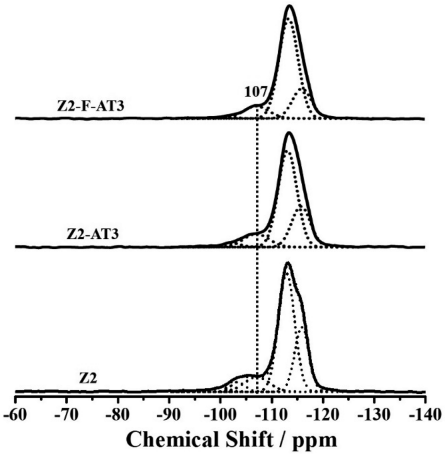

Figure 8. ^{29}Si MAS NMR spectra of parent Z2, TPAOH treated Z2-AT3, and sequential NH_4F-TPAOH treated Z2-F-AT3.

DOI: 10.1021/acs.iecr.8b03539
Ind. Eng. Chem. Res. 2018, 57, 15375−15384

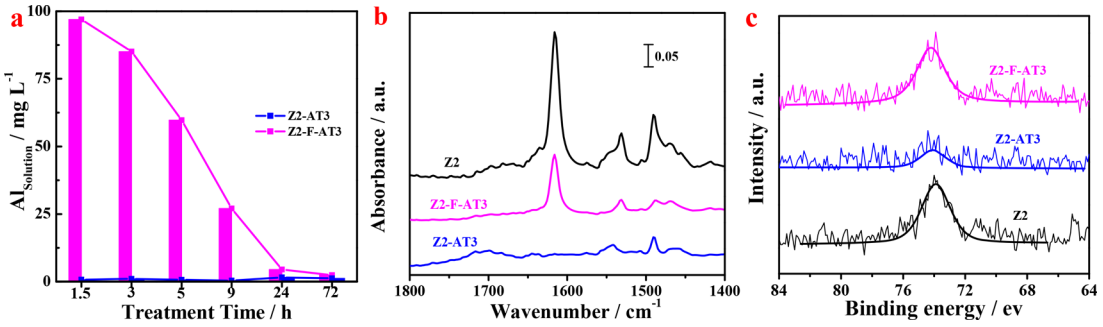

Figure 9. **a**. Al contents in the alkaline filtration after various TPAOH treatment times by ICP results; **b**. 2,6-di-*tert*-butylpyridine IR results for Z2, Z2-AT3, and Z2-F-AT3 at 423 K; and **c**. Al 2p XPS spectra of different samples.

compared with parent Z2, corresponding with slightly larger amounts of acid sites (NH_3-TPD results, Figure 7a).

3.2.3. Influence on Si and Al Redistribution. The influence of various Al coordinates on T atoms redistribution during TPAOH treatment was studied by ICP, 2,6-di-*tert*-butylpyridine IR, and XPS. The variation of Al concentration in the filtrate during TPAOH treatment is shown in Figure 9a. There was a consistent and very low concentration of Al in the filtrate for parent Z2 throughout the treatment process. In contrast, a higher concentration of Al was observed for Z2-F-AT3 in the initial 1.5 h, and those removed Al sites gradually deposited on zeolites as TPAOH treatment time extension, similar to the dealumination-realumination process during NaOH treatment of Z1-F or Z1-Steam. However, by analysis of NH_3-TPD, ^{29}Si MAS NMR, and OH-IR results of Z2-F-AT3, one can draw a conclusion that those deposited Al sites during TPAOH treatment served as framework four-coordinate Al sites, corresponding with larger amounts of acid sites from NH_3-TPD results (Figure 7a), which differed from those deposited Al sites (acidless sites) during NaOH treatment. The external surface acidity of different samples was analyzed by 2,6-di-*tert*-butylpyridine IR. As shown in Figure 9b, Z2 exhibited the largest 2,6-di-*tert*-butylpyridine adsorption peak at 1610 cm^{-1} that represented the largest amounts of Brönsted acid sites at the external surface.[57] Interestingly, the FT-IR spectrum of Z2-AT3 displayed no 2,6-di-*tert*-butylpyridine adsorption peak at 1610 cm^{-1} that indicated a few Brönsted acid sites at the external surface. Thus, it can be concluded that hollow Z2-AT3 had an ultrasilica outer shell, which is confirmed by the XPS results in Figure 9c. TPAOH selectively removed a defective Si-richer interior that resulted in a hollow structure. Moreover, a few Al sites were extracted into the alkaline solution; finally, only desilication and Si-recrystallization occurred with Z2-AT3 during TPAOH treatment. So, selectively removed Si from a Si-richer interior recrystallized onto the outer surface and yielded an ultrasilica outer shell. Figure S6 showed SEM images of ZSM-5 with different Si/Al using TPAOH as a template. The morphology shifted from ellipsoidal type to prismatic type with increasing Si/Al, and Z2-AT3 showed similar prismatic morphology as ZSM-5 with higher Si/Al. Z2-F-AT3 displayed a smaller 2,6-di-*tert*-butylpyridine adsorption peak at 1610 cm^{-1}, indicating a high-silica outer surface compared with parent Z2. However, it exhibited many more external Brönsted acid sites than Z2-AT3, because of additional dealumination and Al-recrystallization processes.

3.3. Catalytic Performance of Samples with Various Hierarchical Structure and T Atoms Distribution. Figure 10 and Table 3 showed the catalytic performance of Z1, Z1-AT1, Z1-Steam-AT1, Z1-F-AT1, and Z1-AT2 in the MTP reaction. Parent Z1 showed a lifetime of 36 h, and Z1-AT1 via NaOH treatment showed a longer lifetime of 124 h, which was attributed to the mesoporous structure after alkaline treatment that facilitated the diffusion of larger precursors and enhanced coke tolerance.[58,59] Z1-F-AT1 and Z1-Steam-AT1 via sequential fluorination/steaming and NaOH treatment showed much longer lifetimes of 148 and 156 h, respectively. As shown in Figure S2, Z1-AT1 showed a larger amount of acid sites compared with Z1-F-AT1 and Z1-Steam-AT1. According to a previous study, the lower the Si/Al (larger amounts of acid sites), the faster the formation rate of methylated aromatic species, finally resulting in a higher coke deposition rate.[60] The lifetime of mesoporous Z1-AT2 increased by only 19 h, and because Z1-AT2 had an intact outer surface, the coke precursors still passed through micropores.[51]

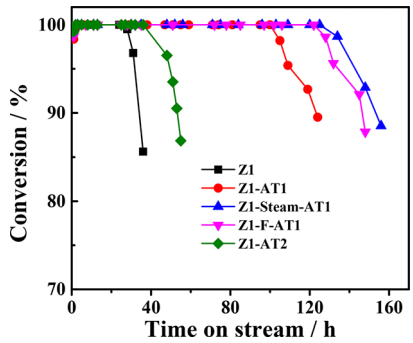

Figure 10. Catalytic performance of parent Z1 and modified samples.

Table 3. Average Product Selectivity of Different Samples

	selectivity/%						
catalysts	CH_4	C_2H_4	C_3H_6	C_4H_8	C_2–C_4	C_5	C_{6+}
Z1	3.52	15.30	32.21	18.02	11.13	15.48	4.34
Z1-AT1	1.76	11.97	40.01	14.86	9.92	16.00	5.48
Z1-F-AT1	1.03	9.27	45.45	13.56	9.17	16.14	5.38
Z1-Steam-AT1	1.09	10.51	44.61	14.10	9.18	16.19	4.32
Z1-AT2	1.53	12.73	37.22	16.92	9.60	17.05	4.95

As shown in Table 3, Z1-AT1 showed a higher propylene selectivity compared with parent Z1. As is known, there were two cycles running simultaneously during the MTH reaction over ZSM-5, aromatics-based and olefins-based reactions. Ethylene was a product of the aromatic-based reaction, and the olefins-based reaction produced propylene and C_{3+} olefins.[61] Introducing an additional mesoporous structure

DOI: 10.1021/acs.iecr.8b03539
Ind. Eng. Chem. Res. 2018, 57, 15375−15384

reduced the resident time of polymethylbenzene in the micropores, which weakened aromatic based reactions but increased olefin-based reactions, resulting in higher propylene selectivity and lower ethylene selectivity.[62,63] Z1-AT1 showed higher propylene selectivity/ethylene selectivity (P/E) of 3.34 compared with Z1 (2.10). The acid amount also influenced the product selectivity. The fewer acid sites weakened aromatic-based reactions and increased the proportion of olefin-based reactions, finally resulting in higher propylene selectivity and P/E.[64] Thus, Z1-F-AT1 and Z1-Steam-AT1 with mesoporous structures and fewer amounts of acid sites showed much higher propylene selectivity and P/E compared with Z1-AT1. Z1-AT2 showed a slightly lower propylene selectivity compared with Z1-AT2.

Z2, Z2-AT3, and Z2-F-AT3 with different T atoms distribution and hierarchical structure were evaluated in a methanol-to-propylene reaction. As shown in Figure 11a, the

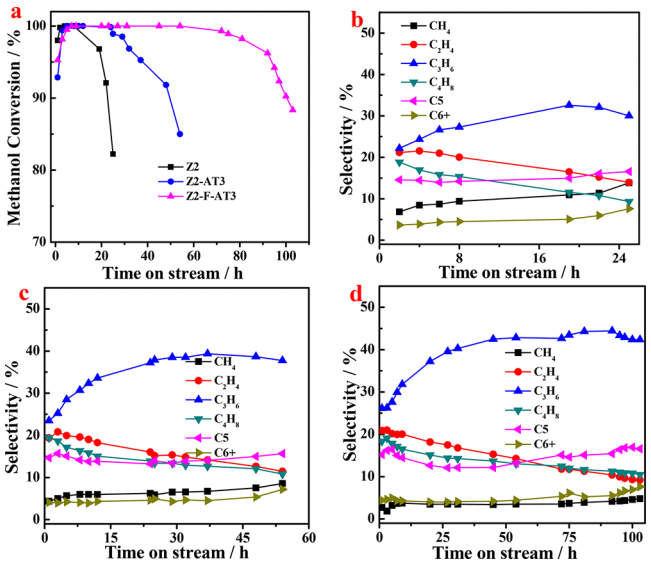

Figure 11. Catalytic performance of Z2, Z2-AT3, and Z2-F-AT3 in the MTP reaction: **a**. methanol conversion versus time on stream and **b**, **c**, **d**. product distribution of Z2, Z2-AT3, and Z2-F-AT3, respectively. (Temperature = 773 K, H_2O/CH_3OH molar ratio was 1, and methanol WHSV = 3.4 h^{-1}.)

methanol conversion over Z2 dropped below 90% within 20 h TOS, because large amounts of acid sites at the external surface led to faster coke deposition at the external surface that blocked the entrances of micropores. TPAOH treatment of Z2-AT3 resulted in hollow ZSM-5 with an ultrasilica outer surface by Si redistribution, which also facilitated the diffusion rate of coke precursors by shortening micropores,[13] restricting coke deposition onto the pore mouth by nonselective coke reactions.[65−67] Both of the factors resulted in a longer lifetime, but the enclosed hollow structure was still not conducive enough to the diffusion of large coke precursors and restricted further improvement of lifetime.[34,51] Hierarchical Z2-F-AT3 with a larger mesopore area and a high-silica outer surface was obtained by Si and Al redistribution during TPAOH treatment, which significantly enhanced the diffusion rate of coke precursors, explaining a much longer lifetime of Z2-F-AT3. Figure 12 showed TGA and TG curves of different catalysts after various reaction times. The weight loss between 750 and 950 K in air atmosphere represented coke combustion. Within

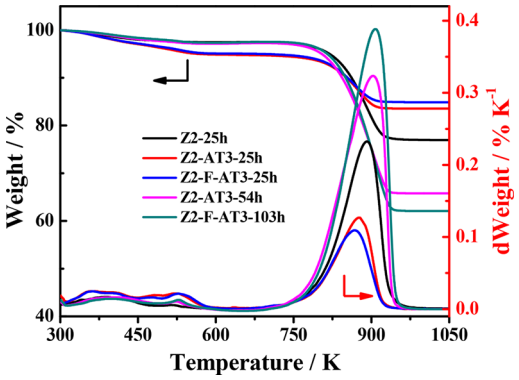

Figure 12. TG curves of Z2, Z2-AT3, and Z2-F-AT3 with various reaction times in MTP reactions.

the same reaction time (25 h), coke amounts decreased as follows: Z2 > Z2-AT3 > Z2-F-AT3. Z2 displayed the largest amounts of coke that was attributed to the acid-richer external surface, while Z2-AT3 with an ultrasilica outer surface significantly decreased the coke deposition rate within 25 h. Z2-F-AT3 with larger amounts of external acid sites but larger amounts of mesopores showed a slightly lower coke amount compared with Z2-AT3 within 25 h, and Z2-F-AT3 exhibited 10% and 38% coke amounts at 25 and 103 h, respectively. It can be speculated that hierarchical Z2-F-AT3 showed a relatively stable coke deposition rate. By contrast, Z2-AT3 showed 13% and 33% coke amounts at 25 and 54 h, respectively. It can be inferred that faster deactivation occurred in the final reaction stage, because intrinsic micropores were more and more unconducive for the diffusion of coke precursors with reaction time extension.

The selectivity versus time on stream over various catalysts is shown in Figure 11**b**, 11**c**, and 11**d**. Parent Z2 displayed similar ethylene and propylene selectivity in the initial stage. The propylene selectivity increased from initial 22.16% to final 30.04% with an average selectivity of 27.88% (Table 4). By

Table 4. Average Products Distribution from the Whole Reactions for Different Catalysts

	selectivity/%						
catalysts	CH_4	C_2H_4	C_3H_6	C_4H_8	C_2–C_4	C_5	C_{6+}
Z2	9.93	18.49	27.88	14.10	9.65	14.96	4.99
Z2-AT3	6.23	16.67	33.98	14.73	9.43	14.34	4.62
Z2-F-AT3	3.66	14.85	38.32	13.89	9.32	14.80	5.16

contrast, ethylene selectivity reduced to 13.94% in the final stage with an average selectivity of 18.49%. As is known, there have been two cycles running simultaneously during the MTH reaction over ZSM-5, aromatics-based and olefins-based reactions.[61,68] In the initial stage of reaction, large amounts of acid sites facilitated aromatics-based reactions that resulted in higher ethylene selectivity.[64] With more and more active sites covered by coke as reaction time extension, the aromatics-based reactions weakened, finally resulting in lower ethylene selectivity but higher propylene selectivity. Z2 showed an initial higher methane selectivity of 6.85%, finally increasing to 13.83% with a higher average selectivity of 9.93%. According to a previous study, methane selectivity was closely associated with diffusion.[69] Z2-AT3 with a hollow structure shortened diffusion path gives lower average methane selectivity of 6.23%

DOI: 10.1021/acs.iecr.8b03539
Ind. Eng. Chem. Res. 2018, 57, 15375−15384

(Table 4). Significantly reduced methane selectivity of 3.66% was obtained over Z2-F-AT3 with a mesoporous structure. Z2-F-AT3 with a mesoporous structure showed a higher average propylene selectivity of 38.32% compared with Z2 (27.88%) and Z2-AT3 (33.98%) and the lowest ethylene selectivity of 14.85% among the three catalysts.

By comparing the catalytic performance of the two kinds of samples in the MTP reaction, we can conclude that (1) Introducing mesopores into ZSM-5 significantly enhanced catalytic stability and propylene selectivity, however, the enclosed mesoporous structure contributed less to the improvement of catalytic performance; (2) Alkaline treatment influenced porosity and acidity, and both of the factors determined catalytic performance. Sequential treatment combined porosity and acidity modulation, finally resulting in superior catalytic performance; (3) By comparing the catalytic performance of Z1, Z2, and Z2-AT3, it can be concluded that samples with less external acid sites showed a longer lifetime. Generally speaking, ZSM-5 with an opened mesoporous structure, a suitable amount of acid sites, and less external acid sites may show superior catalytic performance in the MTP reaction.

4. CONCLUSIONS

Various Al coordinates showed different influence on hierarchical structure and T atoms redistribution during base leaching. Only the desilication process occurred with ZSM-5 with only framework four-coordinate Al species during NaOH treatment, but it involved an additional Si-recrystallization process during TPAOH treatment. While dealumination, realumination, and desilication processes occurred with ZSM-5 with extra-framework Al species during NaOH treatment, redistributed Al sites contributed less to acidity; dealumination, desilication, and (Si, Al)-recrystallization processes occurred during TPAOH treatment, and by contrast, those redistributed Al sites served as framework four-coordinate Al.

For Al-zoned ZSM-5 with only framework Al, TPAOH treatment resulted in hollow structures with an ultrasilica shell, which exhibited a longer lifetime of 50 h in the MTP reaction compared with parent ZSM-5 (20 h) by decreasing external coke deposition. Sequential NH_4F and TPAOH treatment of Al-zoned ZSM-5 involved both Si and Al atoms redistribution. As a result, the mesoporous structure with a high-silica outer surface instead of enclosed cavities was obtained, which resulted in a longer lifetime of 100 h in the MTP reaction. It also showed a high solid yield of 91% and similar crystallinity to parent ZSM-5. This work resulted in a further understanding of the desilication mechanism and proposed a method to design superior catalysts.

■ ASSOCIATED CONTENT

Supporting Information

The Supporting Information is available free of charge on the ACS Publications website at DOI: 10.1021/acs.iecr.8b03539.

Sample list; ^{27}Al MAS NMR spectra of Z1, Z1-F, Z1-Steam, and Z2; NH_3-TPD results of parent Z1 and modified Z1; Ar adsorption−desorption isotherms and pore size distribution curves of Z2, Z2-F, Z2-AT3, and Z2-F-AT3; ^{29}Si MAS NMR spectra of Z2-F; SEM images of ZSM-5 with different Si/Al ratios (PDF)

■ AUTHOR INFORMATION

Corresponding Authors

*Fax: +86 0411 84986134. E-mail: lium@dlut.edu.cn.
*Fax: +1 814 863 4466. E-mail: csong@psu.edu.

ORCID

Min Liu: 0000-0003-2291-6266
Xinwen Guo: 0000-0002-6597-4979
Chunshan Song: 0000-0003-2344-9911

Notes

The authors declare no competing financial interest.

■ ACKNOWLEDGMENTS

The authors acknowledge the financial support of the National Key Research and Development Program of China (No. 2018YFB0604801).

■ REFERENCES

(1) Corma, A. Inorganic Solid Acids and Their Use in Acid-Catalyzed Hydrocarbon Reactions. *Chem. Rev.* **1995**, *95*, 559−614.
(2) Corma, A. From Microporous to Mesoporous Molecular Sieve Materials and Their Use in Catalysis. *Chem. Rev.* **1997**, *97*, 2373−2420.
(3) Smit, B.; Maesen, T. L. M. Molecular Simulations of Zeolites: Adsorption, Diffusion, and Shape Selectivity. *Chem. Rev.* **2008**, *108*, 4125−4184.
(4) Zheng, A.; Huang, S.-J.; Liu, S.-B.; Deng, F. Acid Properties of Solid Acid Catalysts Characterized by Solid-State ^{31}P NMR of Adsorbed Phosphorous Probe Molecules. *Phys. Chem. Chem. Phys.* **2011**, *13*, 14889−14901.
(5) Zheng, A.; Zhang, H.; Lu, X.; Liu, S.-B.; Deng, F. Theoretical Predictions of ^{31}P NMR Chemical Shift Threshold of Trimethylphosphine Oxide Absorbed on Solid Acid Catalysts. *J. Phys. Chem. B* **2008**, *112*, 4496−4505.
(6) Zheng, A.; Liu, S.-B.; Deng, F. ^{31}P NMR Chemical Shifts of Phosphorus Probes as Reliable and Practical Acidity Scales for Solid and Liquid Catalysts. *Chem. Rev.* **2017**, *117*, 12475−12531.
(7) Zheng, A.; Li, S.; Liu, S.-B.; Deng, F. Acidic Properties and Structure−Activity Correlations of Solid Acid Catalysts Revealed by Solid-State NMR Spectroscopy. *Acc. Chem. Res.* **2016**, *49*, 655−663.
(8) Perez-Ramirez, J.; Christensen, C. H.; Egeblad, K.; Christensen, C. H.; Groen, J. C. Hierarchical Zeolites: Enhanced Utilisation of Microporous Crystals in Catalysis by Advances in Materials Design. *Chem. Soc. Rev.* **2008**, *37*, 2530−2542.
(9) Beck, J. S.; Vartuli, J. C.; Roth, W. J.; Leonowicz, M. E.; Kresge, C. T.; Schmitt, K. D.; Chu, C. T. W.; Olson, D. H.; Sheppard, E. W.; McCullen, S. B.; Higgins, J. B.; Schlenker, J. L. A New Family of Mesoporous Molecular Sieves Prepared with Liquid Crystal Templates. *J. Am. Chem. Soc.* **1992**, *114*, 10834−10843.
(10) Zhao, D.; Feng, J.; Huo, Q.; Melosh, N.; Fredrickson, G. H.; Chmelka, B. F.; Stucky, G. D. Triblock Copolymer Syntheses of Mesoporous Silica with Periodic 50 to 300 Angstrom Pores. *Science* **1998**, *279*, 548.
(11) Gao, D.; Duan, A.; Zhang, X.; Chi, K.; Zhao, Z.; Li, J.; Qin, Y.; Wang, X.; Xu, C. Self-Assembly of Monodispersed Hierarchically Porous Beta-SBA-15 with Different Morphologies and Its Hydro-Upgrading Performances for Fcc Gasoline. *J. Mater. Chem. A* **2015**, *3*, 16501−16512.
(12) Shi, J.; Wang, Y.; Yang, W.; Tang, Y.; Xie, Z. Recent Advances of Pore System Construction in Zeolite-Catalyzed Chemical Industry Processes. *Chem. Soc. Rev.* **2015**, *44*, 8877−8903.
(13) Mintova, S.; Gilson, J.-P.; Valtchev, V. Advances in Nanosized Zeolites. *Nanoscale* **2013**, *5*, 6693−6703.
(14) Shen, K.; Qian, W.; Wang, N.; Su, C.; Wei, F. Centrifugation-Free and High Yield Synthesis of Nanosized H-ZSM-5 and Its Structure-Guided Aromatization of Methanol to 1,2,4-Trimethylbenzene. *J. Mater. Chem. A* **2014**, *2*, 19797−19808.

DOI: 10.1021/acs.iecr.8b03539
Ind. Eng. Chem. Res. 2018, 57, 15375−15384

(15) Estermann, M.; McCusker, L. B.; Baerlocher, C.; Merrouche, A.; Kessler, H. A Synthetic Gallophosphate Molecular Sieve with a 20-Tetrahedral-Atom Pore Opening. *Nature* **1991**, *352*, 320.
(16) Merrouche, A.; Patarin, J.; Kessler, H.; Soulard, M.; Delmotte, L.; Guth, J. L.; Joly, J. F. Synthesis and Characterization of Cloverite: A Novel Gallophosphate Molecular Sieve with Three-Dimensional 20-Membered Ring Channels. *Zeolites* **1992**, *12*, 226−232.
(17) Lopez-Orozco, S.; Inayat, A.; Schwab, A.; Selvam, T.; Schwieger, W. Zeolitic Materials with Hierarchical Porous Structures. *Adv. Mater.* **2011**, *23*, 2602−2615.
(18) Möller, K.; Bein, T. Mesoporosity - a New Dimension for Zeolites. *Chem. Soc. Rev.* **2013**, *42*, 3689−3707.
(19) Valtchev, V.; Majano, G.; Mintova, S.; Perez-Ramirez, J. Tailored Crystalline Microporous Materials by Post-Synthesis Modification. *Chem. Soc. Rev.* **2013**, *42*, 263−290.
(20) Choi, M.; Na, K.; Kim, J.; Sakamoto, Y.; Terasaki, O.; Ryoo, R. Stable Single-Unit-Cell Nanosheets of Zeolite MFI as Active and Long-Lived Catalysts. *Nature* **2009**, *461*, 246−249.
(21) Xu, D.; Ma, Y.; Jing, Z.; Han, L.; Singh, B.; Feng, J.; Shen, X.; Cao, F.; Oleynikov, P.; Sun, H.; Terasaki, O.; Che, S. Π−Π Interaction of Aromatic Groups in Amphiphilic Molecules Directing for Single-Crystalline Mesostructured Zeolite Nanosheets. *Nat. Commun.* **2014**, *5*, 4262.
(22) Choi, M.; Cho, H. S.; Srivastava, R.; Venkatesan, C.; Choi, D.-H.; Ryoo, R. Amphiphilic Organosilane-Directed Synthesis of Crystalline Zeolite with Tunable Mesoporosity. *Nat. Mater.* **2006**, *5*, 718.
(23) Cho, K.; Cho, H. S.; de Ménorval, L.-C.; Ryoo, R. Generation of Mesoporosity in LTA Zeolites by Organosilane Surfactant for Rapid Molecular Transport in Catalytic Application. *Chem. Mater.* **2009**, *21*, 5664−5673.
(24) Na, K.; Choi, M.; Park, W.; Sakamoto, Y.; Terasaki, O.; Ryoo, R. Pillared MFI Zeolite Nanosheets of a Single-Unit-Cell Thickness. *J. Am. Chem. Soc.* **2010**, *132*, 4169−4177.
(25) Bai, P.; Wu, P.; Xing, W.; Liu, D.; Zhao, L.; Wang, Y.; Xu, B.; Yan, Z.; Zhao, X. S. Synthesis and Catalytic Properties of ZSM-5 Zeolite with Hierarchical Pores Prepared in the Presence of N-Hexyltrimethylammonium Bromide. *J. Mater. Chem. A* **2015**, *3*, 18586−18597.
(26) Wang, H.; Pinnavaia, T. J. MFI Zeolite with Small and Uniform Intracrystal Mesopores. *Angew. Chem., Int. Ed.* **2006**, *45*, 7603−6.
(27) Xiao, F. S.; Wang, L.; Yin, C.; Lin, K.; Di, Y.; Li, J.; Xu, R.; Su, D. S.; Schlogl, R.; Yokoi, T.; Tatsumi, T. Catalytic Properties of Hierarchical Mesoporous Zeolites Templated with a Mixture of Small Organic Ammonium Salts and Mesoscale Cationic Polymers. *Angew. Chem., Int. Ed.* **2006**, *45*, 3090−3.
(28) Schmidt, I.; Boisen, A.; Gustavsson, E.; Ståhl, K.; Pehrson, S.; Dahl, S.; Carlsson, A.; Jacobsen, C. J. H. Carbon Nanotube Templated Growth of Mesoporous Zeolite Single Crystals. *Chem. Mater.* **2001**, *13*, 4416−4418.
(29) Chen, H.; Wydra, J.; Zhang, X.; Lee, P. S.; Wang, Z.; Fan, W.; Tsapatsis, M. Hydrothermal Synthesis of Zeolites with Three-Dimensionally Ordered Mesoporous-Imprinted Structure. *J. Am. Chem. Soc.* **2011**, *133*, 12390−3.
(30) Jacobsen, C. J. H.; Madsen, C.; Houzvicka, J.; Schmidt, I.; Carlsson, A. Mesoporous Zeolite Single Crystals. *J. Am. Chem. Soc.* **2000**, *122*, 7116−7117.
(31) Tao, Y.; Kanoh, H.; Kaneko, K. Zsm-5 Monolith of Uniform Mesoporous Channels. *J. Am. Chem. Soc.* **2003**, *125*, 6044−6045.
(32) Trong On, D.; Kaliaguine, S. Zeolite-Coated Mesostructured Cellular Silica Foams. *J. Am. Chem. Soc.* **2003**, *125*, 618−619.
(33) Verboekend, D.; Perez-Ramirez, J. Design of Hierarchical Zeolite Catalysts by Desilication. *Catal. Sci. Technol.* **2011**, *1*, 879−890.
(34) Kortunov, P.; Vasenkov, S.; Kärger, J.; Valiullin, R.; Gottschalk, P.; Fé Elía, M.; Perez, M.; Stöcker, M.; Drescher, B.; McElhiney, G.; Berger, C.; Gläser, R.; Weitkamp, J. The Role of Mesopores in Intracrystalline Transport in USY Zeolite: PFG NMR Diffusion Study on Various Length Scales. *J. Am. Chem. Soc.* **2005**, *127*, 13055−13059.
(35) Peng, P.; Wang, Y.; Zhang, Z.; Qiao, K.; Liu, X.; Yan, Z.; Subhan, F.; Komarneni, S. ZSM-5-Based Mesostructures by Combined Alkali Dissolution and Re-Assembly: Process Controlling and Scale-Up. *Chem. Eng. J.* **2016**, *302*, 323−333.
(36) Groen, J. C.; Moulijn, J. A.; Pérez-Ramírez, J. Alkaline Posttreatment of MFI Zeolites. From Accelerated Screening to Scale-Up. *Ind. Eng. Chem. Res.* **2007**, *46*, 4193−4201.
(37) Ogura, M.; Shinomiya, S.-y.; Tateno, J.; Nara, Y.; Nomura, M.; Kikuchi, E.; Matsukata, M. Alkali-Treatment Technique — New Method for Modification of Structural and Acid-Catalytic Properties of ZSM-5 Zeolites. *Appl. Catal., A* **2001**, *219*, 33−43.
(38) Groen, J. C.; Peffer, L. A. A.; Moulijn, J. A.; Pérez-Ramírez, J. Mechanism of Hierarchical Porosity Development in MFI Zeolites by Desilication: The Role of Aluminium as a Pore-Directing Agent. *Chem. - Eur. J.* **2005**, *11*, 4983−4994.
(39) Groen, J. C.; Caicedo-Realpe, R.; Abelló, S.; Pérez-Ramírez, J. Mesoporous Metallosilicate Zeolites by Desilication: On the Generic Pore-Inducing Role of Framework Trivalent Heteroatoms. *Mater. Lett.* **2009**, *63*, 1037−1040.
(40) Groen, J. C.; Moulijn, J. A.; Pérez-Ramírez, J. Desilication: On the Controlled Generation of Mesoporosity in MFI Zeolites. *J. Mater. Chem.* **2006**, *16*, 2121.
(41) Yu, L.; Huang, S.; Miao, S.; Chen, F.; Zhang, S.; Liu, Z.; Xie, S.; Xu, L. A Facile Top-Down Protocol for Postsynthesis Modification of Hierarchical Aluminum-Rich MFI Zeolites. *Chem. - Eur. J.* **2015**, *21*, 1048−54.
(42) Pérez-Ramírez, J.; Verboekend, D.; Bonilla, A.; Abelló, S. Zeolite Catalysts with Tunable Hierarchy Factor by Pore-Growth Moderators. *Adv. Funct. Mater.* **2009**, *19*, 3972−3979.
(43) Verboekend, D.; Perez-Ramirez, J. Desilication Mechanism Revisited: Highly Mesoporous All-Silica Zeolites Enabled through Pore-Directing Agents. *Chem. - Eur. J.* **2011**, *17*, 1137−1147.
(44) Wang, D.; Zhang, L.; Chen, L.; Wu, H.; Wu, P. Postsynthesis of Mesoporous ZSM-5 Zeolite by Piperidine-Assisted Desilication and Its Superior Catalytic Properties in Hydrocarbon Cracking. *J. Mater. Chem. A* **2015**, *3*, 3511−3521.
(45) Liu, H.; Xie, S.; Xin, W.; Liu, S.; Xu, L. Hierarchical ZSM-11 Zeolite Prepared by Alkaline Treatment with Mixed Solution of NaOH and CTAB: Characterization and Application for Alkylation of Benzene with Dimethyl Ether. *Catal. Sci. Technol.* **2016**, *6*, 1328−1342.
(46) Zhang, Y.; Zhu, K.; Duan, X.; Zhou, X.; Yuan, W. The Templating Effect of an Easily Available Cationic Polymer with Widely Separated Charge Centers on the Synthesis of a Hierarchical ZSM-5 Zeolite. *J. Mater. Chem. A* **2014**, *2*, 18666−18676.
(47) Sazama, P.; Wichterlova, B.; Dedecek, J.; Tvaruzkova, Z.; Musilova, Z.; Palumbo, L.; Sklenak, S.; Gonsiorova, O. FTIR and ^{27}Al MAS NMR Analysis of the Effect of Framework Al- and Si-Defects in Micro- and Micro-Mesoporous H-ZSM-5 on Conversion of Methanol to Hydrocarbons. *Microporous Mesoporous Mater.* **2011**, *143*, 87−96.
(48) Zhang, H.; Hu, Z.; Huang, L.; Zhang, H.; Song, K.; Wang, L.; Shi, Z.; Ma, J.; Zhuang, Y.; Shen, W.; Zhang, Y.; Xu, H.; Tang, Y. Dehydration of Glycerol to Acrolein over Hierarchical ZSM-5 Zeolites: Effects of Mesoporosity and Acidity. *ACS Catal.* **2015**, *5*, 2548−2558.
(49) Shen, K.; Wang, N.; Chen, X.; Chen, Z.; Li, Y.; Chen, J.; Qian, W.; Wei, F. Seed-Induced and Additive-Free Synthesis of Oriented Nanorod-Assembled Meso/Macroporous Zeolites: Toward Efficient and Cost-Effective Catalysts for the Mta Reaction. *Catal. Sci. Technol.* **2017**, *7*, 5143−5153.
(50) Li, J.; Liu, M.; Guo, X.; Xu, S.; Wei, Y.; Liu, Z.; Song, C. Interconnected Hierarchical ZSM-5 with Tunable Acidity Prepared by a Dealumination−Realumination Process: A Superior MTP Catalyst. *ACS Appl. Mater. Interfaces* **2017**, *9*, 26096−26106.
(51) Milina, M.; Mitchell, S.; Crivelli, P.; Cooke, D.; Pérez-Ramírez, J. Mesopore Quality Determines the Lifetime of Hierarchically Structured Zeolite Catalysts. *Nat. Commun.* **2014**, *5*, 3922−3931.
(52) Dai, C.; Zhang, A.; Li, L.; Hou, K.; Ding, F.; Li, J.; Mu, D.; Song, C.; Liu, M.; Guo, X. Synthesis of Hollow Nanocubes and

DOI: 10.1021/acs.iecr.8b03539
Ind. Eng. Chem. Res. 2018, 57, 15375−15384

Macroporous Monoliths of Silicalite-1 by Alkaline Treatment. *Chem. Mater.* **2013**, *25*, 4197−4205.
(53) Pagis, C.; Morgado Prates, A. R.; Farrusseng, D.; Bats, N.; Tuel, A. Hollow Zeolite Structures: An Overview of Synthesis Methods. *Chem. Mater.* **2016**, *28*, 5205−5223.
(54) Xu, T.; Zhang, Q.; Song, H.; Wang, Y. Fluoride-Treated H-ZSM-5 as a Highly Selective and Stable Catalyst for the Production of Propylene from Methyl Halides. *J. Catal.* **2012**, *295*, 232−241.
(55) Barbera, K.; Bonino, F.; Bordiga, S.; Janssens, T. V. W.; Beato, P. Structure−Deactivation Relationship for ZSM-5 Catalysts Governed by Framework Defects. *J. Catal.* **2011**, *280*, 196−205.
(56) Burel, L.; Tuel, A. Nanozeolites: New Strategies for Designing Ultra Small Silicalite Crystals with Very Few Framework Defects. *Microporous Mesoporous Mater.* **2013**, *174*, 90−99.
(57) Dai, C.; Zhang, A.; Liu, M.; Guo, X.; Song, C. Hollow ZSM-5 with Silicon-Rich Surface, Double Shells, and Functionalized Interior with Metallic Nanoparticles and Carbon Nanotubes. *Adv. Funct. Mater.* **2015**, *25*, 7479−7487.
(58) Schmidt, F.; Hoffmann, C.; Giordanino, F.; Bordiga, S.; Simon, P.; Carrillo-Cabrera, W.; Kaskel, S. Coke Location in Microporous and Hierarchical ZSM-5 and the Impact on the MTH Reaction. *J. Catal.* **2013**, *307*, 238−245.
(59) Bleken, F. L.; Barbera, K.; Bonino, F.; Olsbye, U.; Lillerud, K. P.; Bordiga, S.; Beato, P.; Janssens, T. V. W.; Svelle, S. Catalyst Deactivation by Coke Formation in Microporous and Desilicated Zeolite H-ZSM-5 During the Conversion of Methanol to Hydrocarbons. *J. Catal.* **2013**, *307*, 62−73.
(60) Mores, D.; Kornatowski, J.; Olsbye, U.; Weckhuysen, B. M. Coke Formation During the Methanol-to-Olefin Conversion: In Situ Microspectroscopy on Individual H-ZSM-5 Crystals with Different Brønsted Acidity. *Chem. - Eur. J.* **2011**, *17*, 2874−2884.
(61) Svelle, S.; Joensen, F.; Nerlov, J.; Olsbye, U.; Lillerud, K.-P.; Kolboe, S.; Bjørgen, M. Conversion of Methanol into Hydrocarbons over Zeolite H-ZSM-5: Ethene Formation Is Mechanistically Separated from the Formation of Higher Alkenes. *J. Am. Chem. Soc.* **2006**, *128*, 14770−14771.
(62) Khare, R.; Bhan, A. Mechanistic Studies of Methanol-to-Hydrocarbons Conversion on Diffusion-Free MFI Samples. *J. Catal.* **2015**, *329*, 218−228.
(63) Khare, R.; Millar, D.; Bhan, A. A Mechanistic Basis for the Effects of Crystallite Size on Light Olefin Selectivity in Methanol-to-Hydrocarbons Conversion on MFI. *J. Catal.* **2015**, *321*, 23−31.
(64) Khare, R.; Liu, Z.; Han, Y.; Bhan, A. A Mechanistic Basis for the Effect of Aluminum Content on Ethene Selectivity in Methanol-to-Hydrocarbons Conversion on HZSM-5. *J. Catal.* **2017**, *348*, 300−305.
(65) Mores, D.; Stavitski, E.; Verkleij, S. P.; Lombard, A.; Cabiac, A.; Rouleau, L.; Patarin, J.; Simon-Masseron, A.; Weckhuysen, B. M. Core−Shell H-ZSM-5/Silicalite-1 Composites: Brønsted Acidity and Catalyst Deactivation at the Individual Particle Level. *Phys. Chem. Chem. Phys.* **2011**, *13*, 15985−15994.
(66) Zhao, X.; Hong, Y.; Wang, L.; Fan, D.; Yan, N.; Liu, X.; Tian, P.; Guo, X.; Liu, Z. External Surface Modification of as-Made ZSM-5 and Their Catalytic Performance in the Methanol to Propylene Reaction. *Chin. J. Catal.* **2018**, *39*, 1418−1426.
(67) Li, N.; Zhang, Y.-Y.; Chen, L.; Au, C.-T.; Yin, S.-F. Synthesis and Application of HZSM-5@Silicalite-1 Core−Shell Composites for the Generation of Light Olefins from CH_3Br. *Microporous Mesoporous Mater.* **2016**, *227*, 76−80.
(68) Ilias, S.; Bhan, A. Tuning the Selectivity of Methanol-to-Hydrocarbons Conversion on H-ZSM-5 by Co-Processing Olefin or Aromatic Compounds. *J. Catal.* **2012**, *290*, 186−192.
(69) Schulz, H. Coking" of Zeolites During Methanol Conversion: Basic Reactions of the MTO-, MTP- and MTG Processes. *Catal. Today* **2010**, *154*, 183−194.

DOI: 10.1021/acs.iecr.8b03539
Ind. Eng. Chem. Res. 2018, 57, 15375−15384